Effective production of orbital quantum entanglement in chaotic quantum dots with nonideal contacts

E. H. Santos and F. A. G. Almeida
Departamento de Física, Universidade Federal de Sergipe, 49100-000 São Cristóvão, Sergipe, Brazil
(Received 24 May 2016; revised manuscript received 6 September 2016; published 27 September 2016)

We study orbital entanglement production in a chaotic quantum dot with two-channel leads by varying the opacity of the contacts in the unitary and orthogonal Wigner-Dyson ensembles. We computed the occurrence probability of entangled states (squared norm) and its concurrence (entanglement level). We also define an entanglement production factor to properly evaluate the entanglement behavior in the system considering effective aspects. The results are numerically obtained through (i) integrations over random matrix ensembles (exact results) for the scenario of one contact ideally fixed and (ii) random matrix simulations for arbitrary contact opacities (sampling). Those outcomes are in mutual agreement and indicate that the optimum effective production of orbital entanglement is achieved when both contacts are ideal and the time-reversal symmetry is broken.

DOI: 10.1103/PhysRevB.94.125441

I. INTRODUCTION

Entanglement is an exclusive intriguing quantum feature and has no correspondent in classical physics [1,2]. One system is said to be entangled if it is uniquely described by one single nonseparable wave function. In other words, it is impossible to represent each particle (or subsystem) individually by a quantum state in an entangled system. It is not easy to actually probe and control entanglement [3] and, besides being highly relevant on its own, it has also been widely investigated as a resource in quantum information processing protocols [4], such as quantum cryptography [5,6], quantum communication [7,8], and quantum simulation [9].

Thereby, developing reliable methods for entanglement production and manipulation in solid state systems is of great interest [10–24]. Special attention has been given to using charge carriers (e.g., electrons) as a resource for entanglement. For instance, the electron entanglement can be used in a circuit element of a quantum information processor allowing the entanglement production to provide the teleportation of qubit states across a chip [25]. Recently, Bell inequality has been studied for electrons separated by 1.3 km [26].

Quantum dots are composed of a metal grain connected to two point contacts through which a current is generated [27]. This setup can be seen as an open cavity (scattering center) attached to two leads (wave guides). A scheme for this model is illustrated in Fig. 1. Experimentally, it takes a lot of effort to actually produce quantum dots featuring a particular shape. For this reason, it is more realistic to deal with generic quantum dots, which can be modeled as chaotic cavities. This framework can be further generalized when one considers nonideal contacts. Thus, the probability for electrons to tunnel through a barrier in the lead is given by its transparency. Moreover, a quantum dot has been proposed as a quantum entangler of electrons in mesoscopic systems [18]. The main idea is that the incoming amplitudes of the two electrons are mixed by the quantum dot (scattering process), producing an output two-electron state that can be either orbitally entangled (one of the electrons is reflected while the other is transmitted) or not (both of them reflected or transmitted). This orbital entanglement has been theoretically investigated in the presence and absence of time-reversal symmetry (TRS) [13,28–30] through a bipartite-entanglement quantifier, such as concurrence [31]. However, because the scattering process is chaotic, the output state is random and the entanglement quantifier has no sense if the entangled state does not occur. The probability that the entangled output state occurs is given by its squared norm. This quantity and its correlation with the concurrence are investigated in previous works [29,30]. However, it is necessary to establish another parameter that takes into account the entanglement production in an effective way, combining simultaneously the squared norm and the concurrence. In this work we present a quantity with this purpose, namely *entanglement production factor*, which embodies a suitable framework to study entanglement generation in the quantum dot. Moreover, it allows us to find a different scenario for optimization of the effective orbital entanglement production that has not been addressed in previous works. The results are numerically obtained by means of integrations over random matrix ensembles (exact results) for the scenario of one contact ideally fixed and through random matrix simulations for arbitrary contact opacities (sampling).

This paper is organized as follows. In Sec. II we introduce the general framework for studying entanglement production in quantum dots. We provide some probabilistic considerations about the quantities involved in the entanglement production in Sec. III. The exact approach is discussed in Sec. IV. In Sec. V we outline the numerical procedure used here. Our main results are shown in Sec. VI and in Sec. VII we draw out our conclusions.

II. PHYSICAL SETUP

We begin with a simple model for a two-lead quantum dot (see Fig. 1) based on Ref. [28]. An electron can tunnel through each contact with a certain rate given by the α-contact transparency Γ_α, with $\alpha = 1$ or 2. The opacity γ_α is then oppositely defined as $\gamma_\alpha = \sqrt{1-\Gamma_\alpha}$. Once the electron reaches the chaotic cavity, it may be reflected to the same lead or transmitted to another.

The scattering matrix (**S** matrix) relates the output amplitudes with the incoming ones and defines how they are

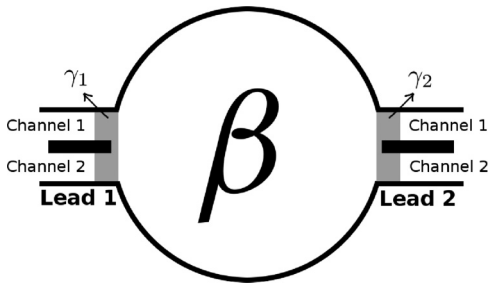

FIG. 1. Schematic drawing of a quantum dot attached to two leads. Each lead features a given opacity value γ. The current can flow when a voltage is applied to the contacts. The circle denotes the scattering chaotic cavity with β symmetry.

distributed in each channel. Note that the $\mathbf{S}$ matrix is unitary [32] ($\mathbf{S}^{-1} = \mathbf{S}^{\dagger}$) since the current must be conserved. This matrix is given from the series association of the three scattering centers of the system, namely contact 1, chaotic cavity, and contact 2, respectively. The chaotic cavity has a corresponding scattering matrix $\mathbf{S}_0$, which is random and governed by the circular Wigner-Dyson ensembles. In this paper we consider two different ensembles: orthogonal ($\beta = 1$) and unitary ($\beta = 2$). The circular orthogonal ensemble represents the electron dynamics in chaotic cavity with time-reversal and spin-rotation invariance, while the unitary circular ensemble is related to the broken time-reversal invariance. The spin-rotation invariance is irrelevant for $\beta = 2$. For $\beta = 1$ the matrix $\mathbf{S}_0$ must also be orthogonal ($\mathbf{S}_0 = \mathbf{S}_0^T$), while for $\beta = 2$ it is solely unitary. The effective $\mathbf{S}$ matrix for the whole system can then be expressed as [33,34]

$$\mathbf{S} = \begin{pmatrix} \mathbf{r} & \mathbf{t}' \\ \mathbf{t} & \mathbf{r}' \end{pmatrix} = \mathbf{R} + \mathbf{T}(\mathbf{1} - \mathbf{S}_0\mathbf{R})^{-1}\mathbf{S}_0\mathbf{T}, \tag{1}$$

where the elements of $\mathbf{r}$ and $\mathbf{t}$ ($\mathbf{r}'$ and $\mathbf{t}'$) are 2×2 blocks of reflection and transmission, respectively, for electrons coming from the left (right) lead. Furthermore, $\mathbf{T} = \mathrm{diag}(t_1,t_1,t_2,t_2)$ and $\mathbf{R} = \mathrm{diag}(r_1,r_1,r_2,r_2)$ stand out as deterministic matrices associated with the contacts, where $r_\alpha = i\gamma_\alpha$ and $t_\alpha = \sqrt{1-\gamma_\alpha^2}$ for contact α. The eigenvalues of the transmission matrix $\mathbf{t}^{\dagger}\mathbf{t}$, τ_1 and τ_2, yield the general properties of quantum transport [27,35].

The entangled output state can be generated if two electrons occupy different leads after the scattering process. The chance that this state occurs is given by its squared norm [29]

$$N = \tau_1 + \tau_2 - 2\tau_1\tau_2. \tag{2}$$

On the other hand, an appropriate entanglement quantifier for this bipartite state is the concurrence [31], which for this system can be expressed by [18]

$$C = 2\frac{\sqrt{(1-\tau_1)\tau_1(1-\tau_2)\tau_2}}{\tau_1 + \tau_2 - 2\tau_1\tau_2}. \tag{3}$$

Furthermore, N and C are correlated through the rule [29] $N(1+C) < 1$. Thereby we can define an entanglement production factor,

$$\eta \equiv NC = 2\sqrt{(1-\tau_1)\tau_1(1-\tau_2)\tau_2}, \tag{4}$$

which provides a better signature for entanglement production, since C does not yield an appropriate description when the output state featuring two electrons occupying different leads does not occur. For instance, if $\tau_1 = \tau_2 = 0$ or 1, $C = 1$, while $N = 0$. In this situation, although the concurrence reaches its maximum value, entanglement is not generated. Indeed, in this case we have $\eta = 0$. On the other hand, if $\tau_1 = 0$ and $\tau_2 = 1$, $C = 0$, while $N = 1$, meaning that the state corresponding to one electron at each lead certainly occurs. However, this state is separable and then, again, there is no entanglement production ($\eta = 0$). Therefore, one can assume that η measures the effective orbital entanglement production. A more detailed interpretation of η is presented in Sec. III.

Due to the chaotic nature of the system, one cannot precisely predict the output state after electrons have gone through the scattering process. Consequently, the transmission eigenvalues are random variables and thus it becomes necessary to perform a statistical analysis of C, N, and η in order to properly understand the entanglement properties of this system. This is carried out in the following sections.

III. PROBABILISTIC CONSIDERATIONS ABOUT THE ENTANGLEMENT PRODUCTION

For a more formal justification of η definition, we rely on the probability theory. First, we consider an output scattered state given by

$$|\mathrm{out}\rangle = A_{20}|2,0\rangle + A_{11}|1,1\rangle + A_{02}|0,2\rangle, \tag{5}$$

where $|n_1,n_2\rangle$ is the normalized state for n_j electrons in the guide j. Alternatively, the state $|\mathrm{out}\rangle$ can also be represented in terms of the occupation in the channels of each guide $|n_{11}n_{12},n_{21}n_{22}\rangle$, with n_{jl} being the number of electrons in the channel l of the guide j (see Fig. 1).

The situation in which there are electrons in only one of the guides corresponds to one of the states $|2,0\rangle = |11,00\rangle$ and $|0,2\rangle = |00,11\rangle$, which are separable.

On the other side, the case in which there is one electron in each guide corresponds to the state $|1,1\rangle$, which is an overlap of the states $|10,10\rangle$, $|10,01\rangle$, $|01,10\rangle$, and $|01,01\rangle$, in which the individual states of each guide are qubits, $|10\rangle$ and $|01\rangle$. Because concurrence is an entanglement quantifier of bipartite states [31], it only measures the entanglement between the orbitals of the two guides when there is only one electron in each guide. Thus, in order to quantify the entanglement of qubits in this system, it is necessary to determine the projection of the total output state onto the state $|1,1\rangle$. Let us denote this projection state by $|\mathrm{qubits}\rangle = |1,1\rangle\langle 1,1|\mathrm{out}\rangle = A_{11}|1,1\rangle$. Notice that $N = |A_{11}|^2$ is the squared norm presented in Eq. (2).

Reference [36] presents a probabilistic interpretation for the concurrence by showing numerically that this quantity can be obtained through a subtraction of probabilities. Below is an overview of this interpretation based on the state $|1,1\rangle$.

To obtain the concurrence of this state one needs a unitary transformation in which

$$\mathbf{U}|1,1\rangle = \sqrt{P_{\mathrm{EC}}}|\mathrm{EC}\rangle + \sqrt{P_{\mathrm{DC}}}|\mathrm{DC}\rangle,$$

where

$$|\mathrm{EC}\rangle = \frac{1}{\sqrt{2}}\left(e^{i\alpha_{\mathrm{EC}}}|10,10\rangle + e^{i\gamma_{\mathrm{EC}}}|01,01\rangle\right), \quad (6)$$

$$|\mathrm{DC}\rangle = \frac{1}{\sqrt{2}}\left(e^{i\alpha_{\mathrm{DC}}}|10,01\rangle + e^{i\gamma_{\mathrm{DC}}}|01,10\rangle\right). \quad (7)$$

Here $|\mathrm{EC}\rangle$ ($|\mathrm{DC}\rangle$) is the state for electrons occupying equivalent (distinct) channels in their respective guides with equal probability. Moreover, α_{EC},γ_{EC},α_{DC}, and γ_{DC} are parameters of the transformation operator $\mathbf{U}$. Notice that $|\mathrm{EC}\rangle$ and $|\mathrm{DC}\rangle$ are maximally entangled ($C = 1$), and for particular values of the parameters of $\mathbf{U}$ those states correspond to Bell states. Then, P_{EC} and P_{DC} are the probabilities related to the states $|\mathrm{EC}\rangle$ and $|\mathrm{DC}\rangle$, respectively. Although there are more than one transformation that satisfy these conditions, the Wooters concurrence C corresponds to the higher value of $|P_{\mathrm{EC}} - P_{\mathrm{DC}}|$ among all possible transformations:

$$C = \max|P_{\mathrm{EC}} - P_{\mathrm{DC}}|.$$

Let us now review this probabilistic interpretation for the quantification of entanglement taking into account that although the state $|1,1\rangle$ is normalized, the projection of the output state results in a nonnormalized state: $|\mathrm{qubits}\rangle = A_{11}|1,1\rangle$. Applying the unitary operation yields

$$\mathbf{U}|\mathrm{qubits}\rangle = A_{11}\mathbf{U}|1,1\rangle = A_{11}\sqrt{P_{\mathrm{EC}}}|\mathrm{EC}\rangle + A_{11}\sqrt{P_{\mathrm{DC}}}|\mathrm{DC}\rangle.$$

Hence, we notice that the probabilities related to the states $|\mathrm{EC}\rangle$ and $|\mathrm{DC}\rangle$ are NP_{EC} and NP_{DC}, respectively. This result can be understood with the fundamentals of probability theory (more specifically, conditional probability).

The probability of a qubit state (one electron in each guide) after scattering occurs is given by $P(\mathrm{qubits}) = ||\mathrm{qubits}\rangle|^2 = |A_{11}|^2 = N$. If this state occurs, then we apply the transformation $\mathbf{U}$ generating an overlap of states with conditional probabilities $P(\mathrm{EC}|\mathrm{qubits}) = P_{\mathrm{EC}}$ and $P(\mathrm{DC}|\mathrm{qubits}) = P_{\mathrm{DC}}$. Therefore, the joint probability of qubit states occurring after scattering and the $\mathbf{U}$ transforms this state to $|\mathrm{EC}\rangle$ is given by

$$P(\mathrm{qubits,DC}) = P(\mathrm{qubits})P(\mathrm{EC}|\mathrm{qubits}) = NP_{\mathrm{EC}}.$$

Similarly, for $\mathbf{U}$ to generate the state $|\mathrm{DC}\rangle$,

$$P(\mathrm{qubits,DC}) = P(\mathrm{qubits})P(\mathrm{DC}|\mathrm{qubits}) = NP_{\mathrm{DC}}.$$

By maximizing the absolute value of subtraction of joint probabilities, it follows that

$$\begin{aligned}\max|P(\mathrm{qubits,EC}) - P(\mathrm{qubits,DC})| &= N\max|P_{\mathrm{DC}} - P_{\mathrm{DC}}| \\ &= NC = \eta.\end{aligned}$$

Notice that since the qubits state is not normalized, the maximization of the absolute value of the subtraction of probabilities did not generate C, as it did for the normalized state $|1,1\rangle$. The following conclusions can be determined by analogy to the considerations of the probability theory: (i) N is the probability of qubits state (one electron in each guide) occurring after scattering, (ii) C is the entanglement factor conditioned to the occurrence of qubits state after scattering, and (iii) $\eta = NC$ corresponds to the joint entanglement factor which involves simultaneously the occurrence of qubits state and how entangled it is. This probabilistic interpretation reinforces the idea presented in the previous section, that is, η is the effective quantifier for the production of the orbital entanglement in this system, which is more convenient than the concurrence, since entanglement only exists if the state of one electron in each guide occurs.

IV. EXACT APPROACH

Let us assume the scenario where one contact is ideal and the other has arbitrary opacity: either $\gamma_1 = 0$ and $\gamma_2 = \gamma$ or $\gamma_1 = \gamma$ and $\gamma_2 = 0$. In this situation, the joint probability density functions (JPDFs) of transmission eigenvalues are known for orthogonal [37] and unitary [30] ensembles. We denote these JPDFs by $P_\gamma^{(\beta)}(\tau_1,\tau_2)$ so that

$$P_\gamma^{(1)}(\tau_1,\tau_2) = \frac{(\gamma^2-1)^8\sum_{i,j=0}^{4}A_{ij}(\gamma)(1-\tau_1)^i(1-\tau_2)^j}{[1-\gamma^2(1-\tau_1)]^6[1-\gamma^2(1-\tau_2)]^6}, \quad (8)$$

where A_{ij} are the elements of the matrix

$$\mathbf{A} = \begin{pmatrix} 0 & 0 & 6 & 12\gamma^2 & 2\gamma^4 \\ 0 & -12 & -12\gamma^2 & 52\gamma^4 & 12\gamma^6 \\ 6 & -12\gamma^2 & -108\gamma^4 & -12\gamma^6 & 6\gamma^8 \\ 12\gamma^2 & 52\gamma^4 & -12\gamma^6 & -12\gamma^8 & 0 \\ 2\gamma^4 & 12\gamma^6 & 6\gamma^8 & 0 & 0 \end{pmatrix}$$

and

$$P_\gamma^{(2)}(\tau_1,\tau_2) = \frac{3}{4}(1-\gamma^2)^5\frac{|\tau_1-\tau_2|}{\sqrt{\tau_1\tau_2}} \times \frac{1+\frac{2}{3}\gamma^2(2-\tau_1-\tau_2)+\gamma^4(1-\tau_1)(1-\tau_2)}{[1-\gamma^2(1-\tau_1)]^{7/2}[1-\gamma^2(1-\tau_2)]^{7/2}}. \quad (9)$$

Using those JPDFs one can obtain the average of an arbitrary function of τ_1 and τ_2, $F(\tau_1,\tau_2)$,

$$\langle F\rangle = \int_0^1\int_0^1 F(\tau_1,\tau_2)P_\gamma^{(\beta)}(\tau_1,\tau_2)d\tau_1 d\tau_2, \quad (10)$$

or its probability density function (PDF), $P(F) = \langle\delta[F - F(\tau_1,\tau_2)]\rangle$,

$$P(F) = \int_0^1\sum_{\widetilde{\tau}_2}\frac{P_\gamma^{(\beta)}(\tau_1,\widetilde{\tau}_2)}{\left|\frac{\partial F(\tau_1,\tau_2)}{\partial\tau_2}\right|_{\tau_2=\widetilde{\tau}_2}}d\tau_1, \quad (11)$$

where $\widetilde{\tau}_2 = \widetilde{\tau}_2(F,\tau_1)$ are the roots of $F = F(\tau_1,\tau_2)$ for fixed τ_1 and F.

Since N, C, and η are functions of τ_1 and τ_2, we compute their averages and PDFs through Eqs. (10) and (11) via numerical integration. One can find analytical results for $P_\gamma^{(1)}(C)$ in Ref. [37]. Moreover, Ref. [30] contains analytical derivations for the JPDF of C and N for $\beta = 2$.

V. NUMERICAL SIMULATION

Since the JPDF of the transmission eigenvalues is unknown for arbitrary γ_1 and γ_2, the exact PDFs of C, N, and η cannot be obtained through the steps outlined in the previous section. However, numerical simulations based on random matrix theory can be useful to overcome this issue with a great

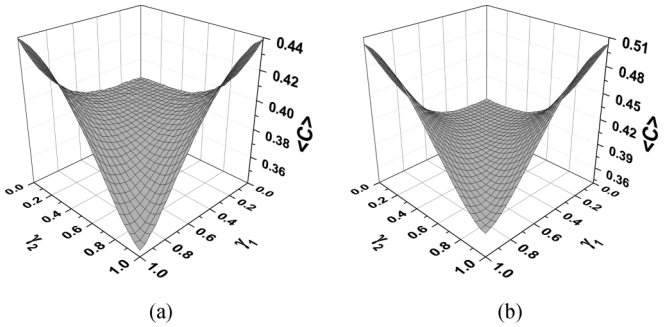

(a) (b)

FIG. 2. Average concurrence versus opacities for (a) $\beta = 1$ and (b) $\beta = 2$.

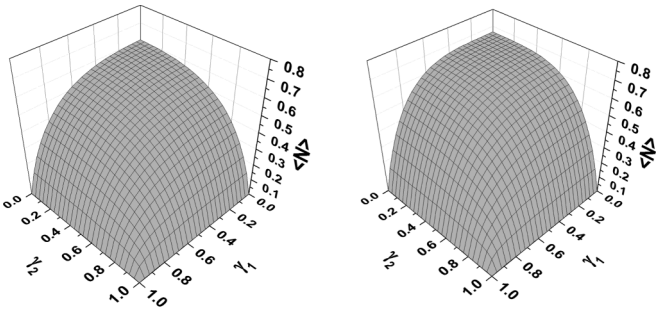

(a) (b)

FIG. 3. Average squared norm versus opacities for (a) $\beta = 1$ and (b) $\beta = 2$.

level of precision and efficiency. In the following, we provide a simple and brief description of the algorithm used for the simulation. A more detailed explanation for this method can be found in Refs. [28,34,38].

The first step is to set the main parameters β, γ_1, and γ_2. Right after that, $\mathbf{S}_0$ is randomly generated by the routine found in Ref. [39]. The $\mathbf{S}$ matrix is obtained through Eq. (1) and then the transmission eigenvalues τ_1 and τ_2 are computed. Using Eqs. (2), (3), and (4) we finally obtain C, N, and η. The corresponding averages and PDFs are extracted through several realizations of this algorithm.

VI. RESULTS AND DISCUSSION

Our results are disposed into three groups. Section VI A presents general results for two contacts with arbitrary opacities while in Sec. VI B we choose one of the contacts to be ideally fixed. In Sec. VI C we discuss the results for symmetric contacts.

A. Contacts with arbitrary opacities

Now we run the protocol described in the previous section, sample-by-sample, in order to discuss the behavior of the concurrence, squared norm, and entanglement factor for different opacity configurations. A similar analysis of the average concurrence for $\beta = 1$ and 2 can be found in Ref. [28].

The behavior of $\langle C \rangle$ is illustrated in Fig. 2. Note that the maximum value of the average concurrence increases with β and it takes place when one contact is opaque and the other is ideal (see Table I). Results for $\langle N \rangle$ are depicted in Fig. 3, which shows that its values increases with β too. Moreover, its maximum occurs for ideal contacts in both β values. A similar feature can be observed in Fig. 4 for $\langle \eta \rangle$, thus indicating that the maximum entanglement production occurs for ideal contacts. Furthermore, Fig. 4 shows that $\langle \eta \rangle$ is greater for a fixed ideal contact than for symmetrical contacts. This feature suggests that in order to carry out a thorough analysis on the maximization of entanglement production, it becomes more appropriate to work along the curve with a single ideal contact.

TABLE I. Maximum values of $\langle C \rangle$, $\langle N \rangle$, and $\langle \eta \rangle$ for $\beta = 1,2$ symmetries including their respective γ_2 value for $\gamma_1 = 0$.

β	$(\gamma_2, \langle C \rangle)$	$(\gamma_2, \langle N \rangle)$	$(\gamma_2, \langle \eta \rangle)$
1	(1,0.44)	(0,0.60)	(0,0.20)
2	(1,0.50)	(0,0.67)	(0,0.23)

B. One ideal contact

Taking into account what was discussed in the previous Sec. VI A, here we consider a single ideal contact and analyze the optimization of entanglement production as we tune the opacity of the other. For simplicity we set $\gamma_1 = 0$ since the physical quantities studied here are invariant under the exchange of the guides. Some properties of this situation are available in Refs. [28–30,37]. This paper is in accordance with their results and includes the analysis of η, which allows us to get more information about the entanglement production.

Figures 5(a) and 5(b) address the behavior of $\langle C \rangle$ and $\langle N \rangle$, respectively. The average concurrence and squared norm take higher values for $\beta = 2$. Note that, regardless of β, the average concurrence (squared norm) reaches its maximum when the second contact is opaque (ideal). It means that most entangled states are prone to occur with lower probabilities. Nevertheless, probability embodies a great significance for an effective entanglement production.

As discussed in Sec. II, η stands out as a convenient parameter as it simultaneously gives us information about the entanglement degree and probability. Its average is shown in Fig. 5(c), at which it is clear that $\langle \eta \rangle$ is a monotonically decreasing function of γ_2 for $\beta = 1$ and $\beta = 2$. Moreover,

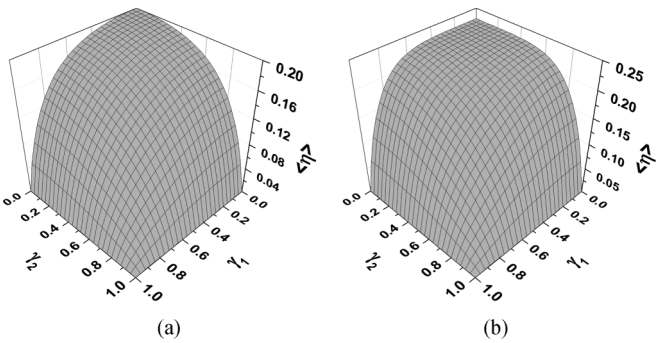

(a) (b)

FIG. 4. Average entanglement factor versus opacities for (a) $\beta = 1$ and (b) $\beta = 2$.

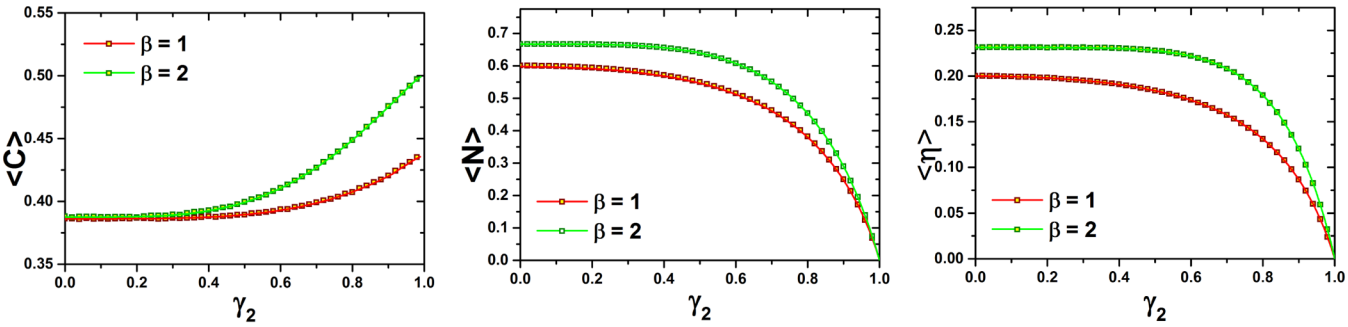

FIG. 5. Averages of (a) concurrence, (b) squared norm, and (c) entanglement production factor versus the opacity of contact 2. Contact 1 is fixed as ideal ($\gamma_1 = 0$). Solid lines represent numerical integration of Eq. (10) while scatter plots address the simulation data.

$\langle C\rangle$, $\langle N\rangle$, and $\langle\eta\rangle$ have higher magnitudes for $\beta = 2$. Thereby breaking the TRS is the best way to drive the entanglement production. Maximum values of $\langle C\rangle$, $\langle N\rangle$, and $\langle\eta\rangle$ are available in Table I.

In order to carry out a more detailed analysis, we also compute the PDFs, which are exposed in Fig. 6 for $\gamma_1 = 0$ in both symmetric cases. From Fig. 6(a) it is clear that the PDF of C becomes more sensitive to γ_2 when $\beta = 2$. Figure 6(b) shows $P(N)$ can assume an irregular shape, especially for $\beta = 1$ and small γ_2 values. The shape of $P(N)$ becomes more regular as β and γ_2 increase. It is worth mentioning there is a singularity when $N = \frac{1}{2}$. This can be predicted theoretically [38] by evaluating N as a function of τ_1 and τ_2 [see Eq. (2)]: a singularity can take place when $\frac{\partial N}{\partial \tau_1} = 0 = \frac{\partial N}{\partial \tau_2}$, implying $\tau_1 = \tau_2 = \frac{1}{2} = N$. Furthermore, Fig. 6(c) shows that the maximum value of η is $\frac{1}{2}$, in agreement with Eq. (4), since η reaches its maximum when $\tau_1 = \tau_2 = \frac{1}{2} = \eta$.

C. Reasonable entanglement production for nonideal contacts

Previously we addressed the scenario of a single ideal contact. Although results show that the maximum entanglement production occurs for two ideal contacts with broken TRS, Fig. 4 shows that $\langle\eta\rangle$ has small variations in regions not so far from its maximum (ideal contacts) for $\beta = 2$. This feature is particularly important since it is difficult to produce ideal contacts. However, a $\langle\eta\rangle$ value near to its maximum (ideal contacts) can be obtained by means of a remarkable decrease in the transparency values of the contacts. For instance, setting $\gamma_1 = \gamma_2 = 0.312$ for broken TRS is equivalent to a 9.73% transparency reduction of the contacts compared to the ideal case ($\Gamma = 1 - \gamma^2$). This configuration produces $\langle\eta\rangle = 0.227$, which represents only 2% loss compared to its highest value. This property can motivate an experimental implementation of the contacts with no major losses in the entanglement production.

In addition to averaging out the quantities of interest, it is also important to check what happens to the PDFs in this situation. Again, we choose $\gamma_1 = \gamma_2 = 0.312$ to perform this analysis. Figure 7 shows the PDFs for C, N, and η compared to the case of ideal contacts. We see that these functions are less sensitive to the opacity from about 0 to 0.327, especially $P(C)$. Considering that the PDF carries full statistical information of a random variable, this feature confirms the good strategy to produce entanglement for nonideal contacts.

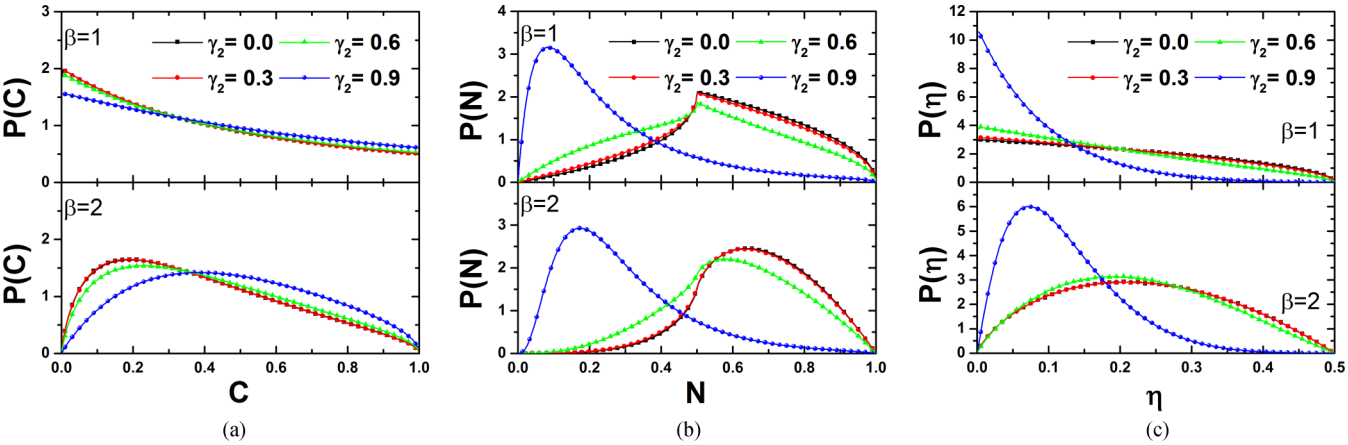

FIG. 6. PDFs of (a) concurrence, (b) squared norm, and (c) entanglement production factor. One of the contacts is ideal ($\gamma_1 = 0$), while the other has an opacity γ_2 represented by the numbers labeling the curves. The two symmetries are in order from top to bottom. Solid lines represent numerical integration of Eq. (11), while scatter plots represent simulation data.

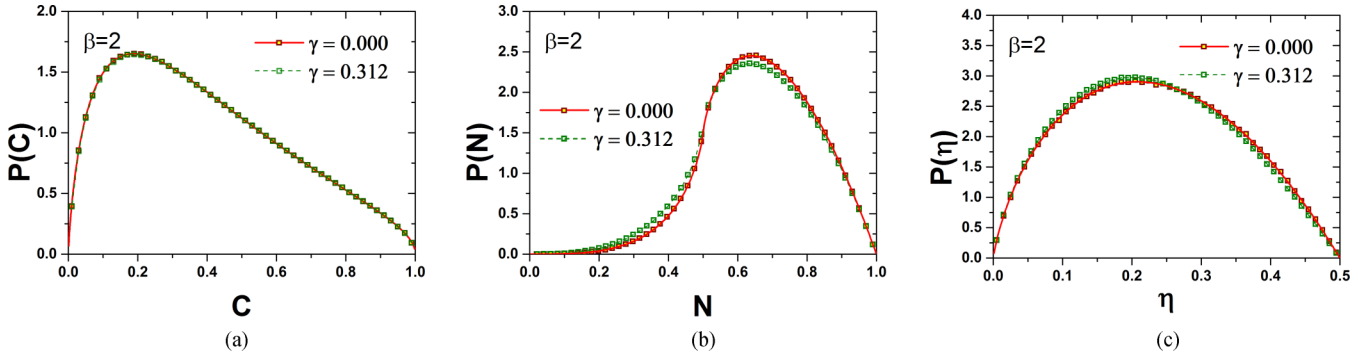

FIG. 7. PDFs of (a) concurrence, (b) squared norm, and (c) entanglement production for $\beta = 2$ and symmetric contacts $\gamma = \gamma_1 = \gamma_2$. Solid lines represent numerical integration of Eq. (11), while scatter plots represent simulation data. Dashed lines are merely guides for the eye.

VII. CONCLUSIONS

We studied the statistics of orbital entanglement production in a chaotic quantum dot with nonideal leads for orthogonal and unitary Wigner-Dyson ensembles. There is a noteworthy agreement between the results obtained through numerical integration (exact results) and simulation (sampling). We showed that the concurrence is maximized when one of the contacts is ideal and the other is opaque, in agreement with a previous work [28]. However, in this situation the transmission eigenvalues are null, $\tau_1 = \tau_2 = 0$, and thus the squared norm and entanglement production factor as well, $N = 0 = \eta$, thereby asserting that entanglement production is not effective in this situation. On the other hand, for $\beta = 1$ and 2, maximum entanglement production occurs when the two contacts are ideal, yielding $\langle\eta\rangle \approx 0.20$ and 0.23, respectively. Therefore, broken TRS is far more efficient for entanglement production. In addition, if the contacts are ideal the entanglement production is barely affected to small variations in the transparency of the contacts. This feature suggests that even for nonideal high-transparency contacts, it is still possible to produce entanglement close to its maximum.

It is important to reinforce that the study presented in this paper is valid for conductors whose phase coherence of charge carriers is preserved. Although it is possible to study quantum transport in systems with few scattering channels in experiments, it is not possible to neglect decoherence effects [40]. Consequently, we believe that an important future work is the study of the properties of orbital entanglement in quantum dots taking into account decoherence effects.

ACKNOWLEDGMENTS

We thank Eugene Kanzieper and Guilherme M. A. Almeida for their attention and helpful tips on the elaboration of the manuscript. This work was supported by CAPES, CNPq and FAPITEC/SE (Brazilian agencies).

[1] G. Alber, T. Beth, P. Horodecki, R. Horodecki, M. Rttler, H. Weinfurter, R. Werner, and A. Zeilinger, *Quantum Information* (Springer, Berlin, 2001), Vol. 173.
[2] M. A. Nielsen and I. L. Chuang, *Quantum Computation and Quantum Information* (Cambridge University Press, Cambridge, 2010).
[3] N. M. Chtchelkatchev, G. Blatter, G. B. Lesovik, and T. Martin, Rev. Phys. B **66**, 161320(R) (2002).
[4] R. Horodecki, P. Horodecki, M. Horodecki, and K. Horodecki, Rev. Mod. Phys. **81**, 865 (2009).
[5] W. Tittel, J. Brendel, H. Zbinden, and N. Gisin, Phys. Rev. Lett. **81**, 3563 (1998).
[6] N. Gisin, G. Ribordy, W. Tittel, and H. Zbinden, Rev. Mod. Phys. **74**, 145 (2002).
[7] H. J. Kimble, Nature (London) **453**, 1023 (2008).
[8] S. Ritter, C. Nölleke, C. Hahn, A. Reiserer, A. Neuzner, M. Uphoff, M. Mücke, E. Figueroa, J. Bochmann, and G. Rempe, Nature (London) **484**, 195 (2012).
[9] I. M. Georgescu, S. Ashhab, and F. Nori, Rev. Mod. Phys. **86**, 153 (2014).
[10] A. M. C. Souza and F. A. G. Almeida, Phys. Rev. A **79**, 052337 (2009).
[11] P. Recher, E. V. Sukhorukov, and D. Loss, Phys. Rev. B **63**, 165314 (2001).
[12] G. B. Lesovik, T. Martin, and G. Blatter, Eur. Phys. J. B **24**, 287 (2001).
[13] V. A. Gopar and D. Frustaglia, Phys. Rev. B **77**, 153403 (2008).
[14] W. D. Oliver, F. Yamaguchi, and Y. Yamamoto, Phys. Rev. Lett. **88**, 037901 (2002).
[15] V. Bouchiat, N. Chtchelkatchev, D. Feinberg, G. B. Lesovik, T. Martin, and J. Torres, Nanotechnology **14**, 77 (2003).
[16] D. S. Saraga and D. Loss, Phys. Rev. Lett. **90**, 166803 (2003).
[17] S. Bose and D. Home, Phys. Rev. Lett. **88**, 050401 (2002).
[18] C. W. J. Beenakker, C. Emary, M. Kindermann, and J. L. van Velsen, Phys. Rev. Lett. **91**, 147901 (2003).
[19] C. W. J. Beenakker, M. Kindermann, C. M. Marcus, and A. Yacoby, in *Fundamental Problems of Mesoscopic Physics*, edited by I. V. Lerner, B. L. Altshuler, and Y. Gefen, NATO Science Series II Vol. 154 (Kluwer, Dordrecht, 2004).
[20] P. Samuelsson, E. V. Sukhorukov, and M. Büttiker, Phys. Rev. Lett. **91**, 157002 (2003).
[21] P. Samuelsson, E. V. Sukhorukov, and M. Büttiker, Phys. Rev. Lett. **92**, 026805 (2004).
[22] A. I. Signal and U. Zlicke, Appl. Phys. Lett. **87**, 102102 (2005).

[23] A. V. Lebedev, G. B. Lesovik, and G. Blatter, Phys. Rev. B **71**, 045306 (2005).
[24] G. Burkard, D. Loss, and E. V. Sukhorukov, Phys. Rev. B **61**, R16303(R) (2000).
[25] R. S. Deacon *et al.*, Nat. Commun. **6**, 7446 (2015).
[26] B. Hensen *et al.*, Nature (London) **526**, 682 (2015).
[27] C. W. J. Beenakker, Rev. Mod. Phys. **69**, 731 (1997).
[28] F. A. G. Almeida and A. M. C. Souza, Phys. Rev. B **82**, 115422 (2010).
[29] S. Rodríguez-Pérez and M. Novaes, Phys. Rev. B **85**, 205414 (2012).
[30] D. Villamaina and P. Vivo, Phys. Rev. B **88**, 041301(R) (2013).
[31] W. K. Wootters, Phys. Rev. Lett. **80**, 2245 (1998).
[32] H. U. Baranger and P. A. Mello, Phys. Rev. Lett. **73**, 142 (1994).
[33] P. W. Brouwer, Phys. Rev. B **51**, 16878 (1995).
[34] F. A. G. Almeida and A. M. S. Macêdo, J. Comput. Phys. **243**, 1 (2013).
[35] Y. V. Nazarov and Y. M. Blanter, *Quantum Transport: Introduction to Nanoscience* (Cambridge University Press, Cambridge, 2009).
[36] A. Sabour and M. Jafarpour, Chin. Phys. Lett. **28**, 070301 (2011).
[37] A. Jarosz, P. Vidal, and E. Kanzieper, Phys. Rev. B **91**, 180203 (2015); A misprint was found on this paper, actually. However, the correct equation for the JPDF has been provided by one of its authors via private message.
[38] F. A. G. Almeida, S. Rodríguez-Pérez, and A. M. S. Macêdo, Phys. Rev. B **80**, 125320 (2009).
[39] K. Życzkowski and M. Kuś, J. Phys. A: Math. Gen. **27**, 4235 (1994).
[40] A. G. Huibers, S. R. Patel, C. M. Marcus, P. W. Brouwer, C. I. Duruöz, and J. S. Harris, Jr., Phys. Rev. Lett. **81**, 1917 (1998).